Spatial Relationship between the Prodan Site, Trp-214, and Cys-34 Residues in Human Serum Albumin and Loss of Structure through Incremental Unfolding†

Shyam Sundar Krishnakumar and Dulal Panda*

Bhupat and Jyoti Mehta School of Biosciences and Bioengineering, Indian Institute of Technology, Bombay, Powai, Mumbai 400 076, India

Received February 19, 2002; Revised Manuscript Received April 16, 2002

ABSTRACT: Prodan (6-propionyl-2-(dimethylamino)-naphthalene), a competitive inhibitor of warfarin binding to human serum albumin (HSA) at drug site I, was used to determine the inter- and intradomain distances of HSA. The fluorescence resonance energy transfer (FRET) distances between prodan and Trp-214, prodan and 7-(diethyl amino)-4-methylcoumarin 3-maleimide (CM)-modified Cys-34, and Trp-214 and CM-Cys-34 were determined to be 25.5 ± 0.5 Å, 33.1 ± 0.8 Å, and 32.4 ± 1 Å, respectively. FRET analysis showed that low concentration of palmitic acid (5 μM) increased the interdomain distance between the Trp-214 in domain II and CM-Cys-34 in domain I by ∼5 Å without perturbing the secondary structure of HSA and the immediate environment of Trp-214. Palmitic acid (5 μM) increased the prodan fluorescence by increasing the quantum yield of bound prodan without altering the tryptophan environment. However, palmitic acid (>10 μM) decreased the prodan fluorescence and increased the tryptophan fluorescence. Our results indicate that the high affinity palmitic acid binding site is located at the interface of domains I and II. On the basis of our measurements, a schematic model representing the drug site-1, Trp-214, and Cys-34 along with the palmitic acid sites has been constructed. In addition, prodan fluorescence, FRET, and ligand binding were used to monitor guanidine hydrochloride-induced denaturation of HSA. An analysis of the equilibrium unfolding data suggests that HSA undergoes a two-state unfolding transition with no detectable intermediate. However, kinetic analysis using multiple probes and thermal denaturation studies showed that the unfolding of the prodan site in HSA preceded the unfolding of tryptophan environment. In addition, the separation of domain I and II occurred before the global unfolding of the protein. The data support the idea that HSA loses its structure incrementally during its unfolding.

Human serum albumin (HSA),[1] a monomeric protein of 585 residues, is the major protein component of blood plasma. It has three structurally similar α-helical domains I−III, which are further divided into subdomains A and B (*1*, *2*). A wide variety of drugs such as warfarin, digitoxin, and benzodiazepine bind to HSA, and much of the interest in this protein derives from its effects on drug delivery (*3*−*6*). The high affinity drug binding sites on HSA have been classified into two well-characterized groups, sites I and II, which are located in subdomains IIA and IIIA, respectively (*1*, *3*). Although examples of drugs binding elsewhere on the protein have been documented (*4*), most work has focused on these primary drug sites. Drug site I, where warfarin binds, has been characterized as a conformationally adaptable region with up to three subcompartments (*5*, *6*).

HSA plays a major role in metabolism and clearance of fatty acid in the body, and the fatty acid binding sites on HSA are distributed throughout the protein involving all six subdomains (*7*, *8*). Under normal physiological conditions, long chain-saturated fatty acids, such as oleate and palmitate, make up almost 70% of the free fatty acid in the blood (*9*). In several disease states, such as bacterial infection, diabetes mellitus, and stress, the fatty acid levels are found to increase remarkably (*10*, *11*). Under such circumstances, the fatty acid modulates the ligand binding properties of HSA by inducing conformational changes in the binding site I and II (*10*−*12*). Thereby, understanding HSA-fatty acid interactions is of major clinical and pharmaceutical importance.

The folding process for a multidomain protein, such as HSA, is complex wherein each domain could fold independently and interdomain interactions regulate the overall folding process (*13*, *14*). Studies on chemically and enzymatically isolated domains of serum albumin have shown that they retain nativelike conformation and ligand binding properties (*15*, *16*). Recently, individual domains (I and III) of HSA have been efficiently expressed and secreted in *Saccharomyces cerevisiae* (*17*), which further confirms that these domains can form independent structural units capable of folding into stable tertiary structure. Several groups examined the mechanism of unfolding of HSA (*18*−*22*). Despite the development of both experimental and theoretical methodologies, no unifying mechanism has been evolved for understanding the unfolding pathways of HSA. Picó (1995) identified a molten globule-like intermediate during the thermal unfolding of HSA (*18*). Acid denaturation studies

† This study was supported by a grant from Indian Institute of Technology, Bombay.

* To whom correspondence should be addressed. Telephone: +91-022-572 7838; FAX: +91-022-572 3480; email: panda@btc.iitb.ac.in.

[1] Abbreviations: HSA, human serum albumin; FRET, fluorescence resonance energy transfer; prodan, 6-propionyl-2-(dimethylamino) naphthalene; CM, 7-(diethyl amino)-4-methylcoumarin 3-maleimide; CM-HSA, CM-labeled HSA.

10.1021/bi025699v CCC: $22.00
Published on Web 05/10/2002

of HSA also indicated the presence of a molten globule-like intermediate at a low pH range (*19*). However, chemical denaturation studies have led to conflicting results on the questions of an intermediate state. Tayyab et al. (1995) examined the urea-induced unfolding of HSA and found that unfolding apparently occurred in a single, concerted step with no intermediate formation (*20*). Recently, Muzammil et al. (2000) found that guanidine hydrochloride (GdnHCl)-induced unfolding occurred in a single step (*21*). However, Flora et al. (1998) reported earlier that the unfolding of HSA by GdnHCl involves multiple steps, with at least one intermediate (*22*). The important issue concerning the unfolding of HSA is whether it is a genuine two-state process or whether the intermediates of unfolding are not detected by thermodynamic or kinetic experiments, as they are too unstable.

HSA contains only one tryptophan residue at position 214 in domain II and one free cysteine residue at position 34 in domain I, although, it has 17 disulfide bonds (*2*, *23*). The free thiol allows site-specific labeling of the protein with chromophoric or fluorescent probes. The intrinsic tryptophan and extrinsic spectroscopic probes at Cys-34 have been used to study ligand-induced conformational changes and the unfolding process of HSA (*12*, *21*, *22*, *24*−*26*). In a multidomain protein, information obtained using a single probe such as tryptophan or prodan reflect the local conformational change but may not be sufficient to characterize the changes occurring in other domains of the protein. HSA contains three domains (*1*, *2*), and it is known that the binding of a ligand at one site in HSA affects the binding of another ligand at a distant site (*25*, *26*). Thus, an analysis involving multiple probes and the changes in spatial distance between these probes could provide more insight into the ligand-induced conformational changes and unfolding process of HSA.

Fluorescence resonance energy transfer (FRET) technique has emerged as a successful tool to determine the spatial distance between two points (a donor and an acceptor) in proteins, and FRET distances between two points have been extensively used to study protein folding pathways, conformational changes upon ligand binding, protein−protein interactions, and monomer−dimer equilibrium (*27*−*30*). In HSA, the FRET distance between Trp-214 and Cys-34 has been used to study chemical unfolding of HSA (*22*) and the effects of pH on HSA structure (*31*).

The environment sensitive hydrophobic fluorescent probes such as 8-anilinonaphthalene-2-sulfonic acid (ANS), bis-ANS, and prodan have been used routinely to monitor protein−ligand interaction, ligand-induced conformational changes in proteins, and unfolding pathways of proteins (*32*−*38*). It has been shown that prodan binds to HSA at single site with high affinity and fluorescence polarization studies demonstrate that the prodan binding site on HSA corresponds to the warfarin-binding site (*38*). Thereby, prodan could be used as a probe for monitoring the drug site I. Binding of prodan to HSA takes place with fluorescence enhancement and a large blue shift that provides an easy separation of the fluorescence contribution from bound and free probe. Further, prodan is very sensitive to the polarity of the environment and could be used to analyze conformational changes associated with ligand binding and unfolding of the structure.

In this report, we have performed FRET analysis of the intra and interdomain distances in HSA and have mapped the prodan binding site in HSA with respect to Trp-214 and 7-(diethyl amino)-4-methylcoumarin 3-maleimide (CM)-modified Cys-34 residues. The spatial relationships among these probes and the environment sensitive prodan fluorescence have been used to study the interactions of palmitic acid with HSA and GdnHCl induced unfolding of HSA. On basis of the above analysis, we characterized the high and low affinity palmitic acid binding sites in HSA. Further, analysis of the equilibrium unfolding data suggested that a two-state model better describes the unfolding behavior than a three-state model, indicating that unfolding of HSA occurs in the absence of any detectable intermediate. However, kinetic analysis using multiple probes and thermal denaturation studies demonstrated that HSA loses its structure through incremental unfolding.

EXPERIMENTAL PROCEDURES

Materials. HSA (essentially fatty acid free) was obtained from National Plasma Fractionation Centre (NPFC), Mumbai, India. The manufacturer employed standard purification and defatting procedures that include several chromatographic steps such as DEAE A-50, Sephadex G-25, DEAE-Sepharose, CM-Sepharose, and Sephacryl S-200 for purifying HSA to homogenity. HSA was found to be >99% pure by Coomassie blue staining of the SDS−PAGE. Prodan [6-propionyl-2-(dimethylamino) naphthalene] and 7-(diethyl amino)-4-methylcoumarin 3-maleimide (CM) were obtained from Molecular Probes Inc. Guanidium hydrochloride (GdnHCl) was from Aldrich Chemical Co., Inc. Palmitic acid was from Sigma Chemical Company. All other chemicals used in the experiments were of analytical grade.

Spectra Measurements. All fluorescence measurements were performed in a JASCO FP-6500 spectrofluorometer at 25 °C equipped with a constant temperature water-circulating bath. Spectra were taken by multiple scans, and buffer blanks were subtracted from all measurements. A quartz cuvette of 0.3-cm path length was used in all experiments to reduce the inner filter effect. The band-pass of both excitation and emission monochromators were 5 nm unless otherwise stated. All absorbance measurements were performed in a JASCO V-530 UV−visible spectrophotometer. The CD spectra were recorded in a JASCO J-810 spectropolarimeter at 25 °C using a 0.5-cm path length cuvette. The spectral data were acquired over the range of 270−190 nm.

Binding of Prodan to HSA. The dissociation constant and stoichiometry of prodan binding to HSA were determined using a double titration procedure (*39*, *40*). Free prodan in aqueous solution has emission maxima centered around 520 nm, and it has negligible fluorescence at 445 nm. Upon binding to HSA, the fluorescence intensity at 445 nm increases severalfolds. HSA (1 μM) was allowed to react with different concentrations of prodan (1 to 30 μM) in 20 mM phosphate buffer (pH 7.0) at 25 °C for 30 min. Increased prodan fluorescence at 445 nm upon binding to HSA was used to determine the affinity of HSA and prodan interaction. The excitation and the emission wavelengths were 360 and 445 nm, respectively. Buffer blank containing different concentrations of prodan was measured and subtracted from the experimental data. We used a 0.3-cm path length fluorescence cell to minimize the inner filter effects. The inner filter effects were corrected empirically by measuring

the absorption of prodan at the excitation and the emission wavelength using the relationship $F_c = F_o$ antilog $[(A_{360} + A_{445})/2]$ (*27*), where F_o is the observed fluorescence, A_{360} is the absorbance of prodan at 360 nm, and A_{445} is the absorbance of prodan at 445 nm. Binding parameters were determined using the relationship 1/[bound prodan] = K_d/n [free prodan] + n, where K_d corresponds to the dissociation constant and n is the binding stoichiometry. The concentration of the bound prodan was determined using the relationship, [bound prodan] = $(F - F_0)/(F_m - F_0)$, where F_0 is the fluorescence intensity of prodan in the absence of HSA, F is the corrected fluorescence intensity when HSA and prodan are in equilibrium, and F_m is the calculated fluorescence intensity of bound prodan. F_m was determined using a reverse titration wherein a fixed concentration of prodan was titrated with increasing amounts of HSA in 20 mM phosphate buffer (pH 7.0) at 25 °C for 30 min. F_m was determined by plotting $1/(F - F_0)$ versus 1/[HSA] and extrapolating 1/[HSA] to zero. The free prodan concentration was calculated as [free prodan] = [total prodan] − [bound prodan].

Acrylamide Quenching Studies. HSA (1 μM) in 20 mM phosphate buffer (pH 7.0) was titrated with increasing concentrations (0−400 mM) of acrylamide at 25 °C. The excitation and emission wavelengths were 295 and 340 nm, respectively. The quenching data were fitted into the Stern−Volmer relationship, $F_o/F = 1 + K_{SV}$ [Q], where F_o is the fluorescence intensity in absence of the quencher, F is the fluorescence intensity in the presence of the quencher, Q is the quencher (acrylamide) concentration, and K_{SV} is the Stern−Volmer quenching constant for collisional quenching.

Chemical Modification of Cys-34. Recently, HSA has been labeled with prodan, acrylodan, and promen in the presence of 8 M urea, and the labeled protein retained its functional properties (*38*, *41*, *42*). We adopted a similar strategy to prepare CM-labeled HSA. For that purpose, we first tested the reversibility of the GdnHCl (6 M) induced denaturation of HSA by removal of GdnHCl by extensive dialysis. Removal of GdnHCl by dialysis resulted in a recovery of the shape of the spectral contour for tryptophan along with the recovery of 95% of the initial fluorescence intensity, and the binding of prodan and palmitic acid to HSA was not affected (data not shown). In addition, the FRET distance between the prodan binding site and Trp-214 was found to be 26.1 ± 0.6 Å, which is similar with the distance measured from the untreated sample. Thus, the denaturation of HSA by GdnHCl was found to be reversible and the denaturation procedure was used to label HSA with CM.

HSA (10 μM) in 20 mM phosphate buffer (pH 7.0) was incubated with 6 M GdnHCl at 25 °C for 4 h and subsequently, 150 μM of CM was added to the reaction mixture. The reaction was quenched after 4 h by addition of excess β-mercaptoethanol, and the excess reagents were removed by exhaustive dialysis for 20 h against 20 mM phosphate buffer (pH 7.0) with buffer changes every 4 h. The incorporation stoichiometry was measured using ϵ_{383} = 30 000 L mol^{-1} cm^{-1} for CM and ϵ_{280} = 36 000 L mol^{-1} cm^{-1} for HSA. HSA concentration was also verified by Bradford method (*43*) using BSA as a standard that yielded similar data. The stoichiometry of CM per mole of HSA was found to be 0.97.

Distance Measurement using Resonance Energy Transfer. Förster's theory of dipole−dipole energy transfer was used to determine the distances between the chromophores (*44*−*46*). By Förster's theory, the efficiency of energy transfer (E) is related to the distance R (Å) between donor and acceptor by

$$E = R_o^6/R_o^6 + R^6 \quad (1)$$

R_o, the distance (Å) at which the transfer efficiency equals to 50%, is given by the following equation

$$R_o = 9.78 \times 10^3 (\kappa^2 \phi_d J \eta^{-4})^{1/6} \quad (2)$$

Where η is the refractive index of the medium, κ^2 is the orientation factor, and ϕ_d is the quantum yield of the donor. The spectral overlap integral (J) between the donor emission spectrum and the acceptor absorbance spectrum was approximated by the following summation,

$$J(\lambda) = \int F_d(\lambda)\epsilon_a(\lambda)\lambda^4 d\lambda / \int F_d(\lambda) d\lambda \quad (3)$$

where $F_d(\lambda)$ and $\epsilon_a(\lambda)$ represent the fluorescence intensity of the donor and the molar extinction coefficient of the acceptor, respectively, at the wavelength λ. The orientation factor, κ^2 was taken to be 2/3, corresponding to isotropic donor and acceptor. It is unlikely that the true value of κ^2 deviates a lot from this value to cause a significant error in R_o calculations. A value for 1.4 was used for refractive index, η. A computer program published earlier was used to calculate the R_o, J, E, and R-values (*47*).

The energy transfer data were obtained by measuring the change in donor fluorescence. The donor fluorescence intensity (F_d) was measured in the absence and presence (F_a) of acceptor. The efficiency of transfer (E) was calculated using eq 4. Since the labeling efficiency was not 100%, the

$$E = 1 - F_a/F_d \quad (4)$$

observed transfer efficiency (E_{obs}) was corrected for the acceptor stoichiometry. The corrected efficiency (E_{cor}) is given as $E_{cor} = E_{obs}/f_a$, where f_a is the fraction of assembly with acceptor (*46*).

Chemical Denaturation Data Analysis. The chemical denaturation data were analyzed using a two-state thermodynamic unfolding model where the transition from native state (N) to unfolded state (U) occurs in the absence of any detectable intermediate. Equations 5−8 describe the thermodynamics of this model.

$$K_U = [U]/[N] \quad (5)$$

$$F[D] = X_N F_N + X_U F_U \quad (6)$$

$$X_U = K_U/1 + K_U; X_N = 1 - X_U \quad (7)$$

$$\Delta G_U = \Delta G_U^\circ - m[D] = -RT \ln K_U \quad (8)$$

K_U is the unfolding equilibrium constant; F[D] is the observed fluorescence intensity at any denaturant concentration [D]; F_N and F_U represent the fluorescence intensity of the native and unfolded state; and X_N and X_U are the mole fractions of the proteins in the native and unfolded state, respectively. ΔG_U and ΔG_U° are the standard free energy changes for the unfolding transition in the presence and

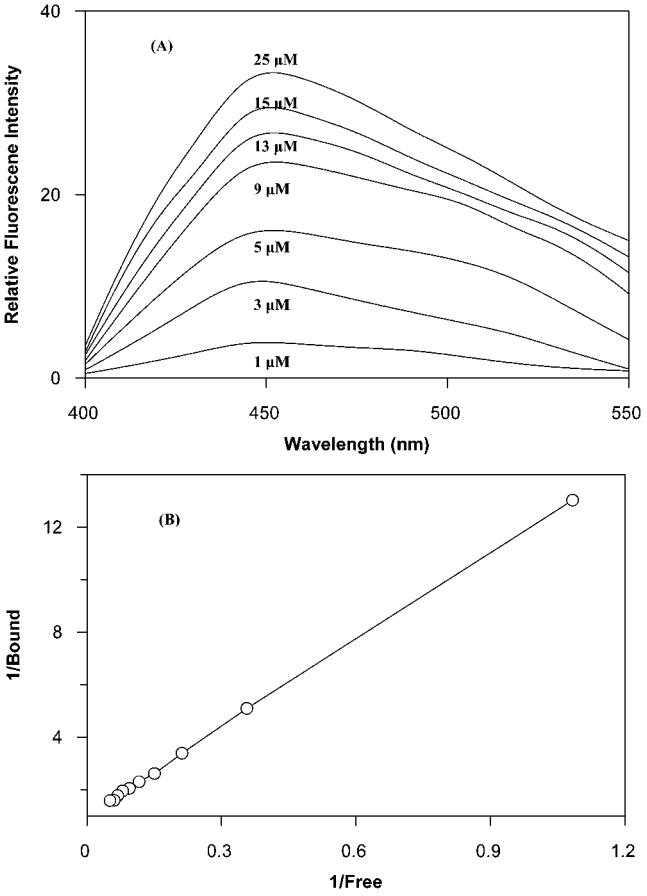

FIGURE 1: Binding of prodan to HSA was determined by fluorescence spectroscopy. (A) HSA (1 μM) was incubated with different concentrations of prodan (0.5−30 μM) at 25 °C for 30 min as described in the Experimental Procedures, and the emission spectra were collected using 360 nm as an excitation wavelength. The prodan concentrations increased from the bottom to top. The fluorescence intensity at 445 nm was used to calculate the concentration of bound prodan. (B) Double reciprocal plot for the binding of prodan to HSA. The binding constant reported is the average of three identical experiments.

absence of denaturant D, and m is the denaturant susceptibility parameter that describes the dependence of ΔG_U on denaturant concentration (*48*). Combining eqs 7 and 8, we get eq 9:

$$X_U = (\exp(m[D] - \Delta G_U^\circ)/RT)/(1 + \exp(m[D] - \Delta G_U^\circ)/RT) \quad (9)$$

The unfolding parameters, ΔG_U° and m, were obtained by a nonlinear regression analysis (Sigma Plot 2001 for Windows) of the data using eq 9.

RESULTS

HSA−Prodan Interaction. The parameters of prodan binding to HSA were obtained using a double titration procedure as described in the Experimental Procedures. Fluorescence of HSA bound prodan increased in a concentration-dependent fashion (Figure 1A), and the analysis of the data in the form of a double reciprocal plot yielded a dissociation constant of $10.9 \pm 0.6 \times 10^{-6}$ M and $n = 1$ (Figure 1B). It has been reported earlier that prodan binds to HSA (*38*) with an association constant of 3.9×10^5 M^{-1} and to bovine serum albumin (*32*) with dissociation constant of 10×10^{-6} M.

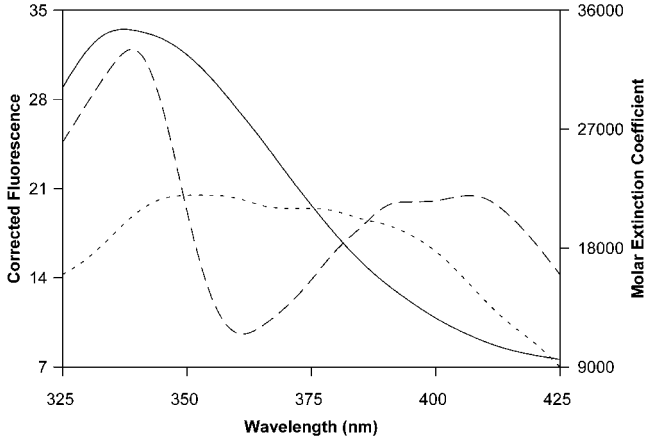

FIGURE 2: Spectral overlaps between the donor Trp-214 emission spectrum (—) was obtained by exciting Trp-214 of HSA at 295 nm and the absorption spectra of acceptors, CM-HSA (— —), and HSA−prodan (- - -) were recorded in 20 mM phosphate buffer, pH 7.0.

Quantum Yield Measurements. We wanted to map the drug site I on HSA with respect to the position of Trp-214 and Cys-34 residues. It was necessary to measure the fluorescence quantum yield (ϕ) of donor chromophores to determine the distance between a donor and acceptor pairs using the Förster's theory of dipole−dipole energy transfer. The relative quantum yields for intrinsic tryptophan in HSA and prodan were determined using tryptophan solution in water ($\phi = 0.14$) and quinine sulfate in 1 N H_2SO_4 ($\phi = 0.55$), respectively, as standard solutions (*44*). The fluorescence quantum yield of Trp-214 was calculated to be 0.19. The quantum yield of bound prodan was calculated to 0.29.

Distance Measurements Between Trp-214 and Prodan Binding Site. The absorption spectrum of prodan extensively overlaps the fluorescence emission of the lone tryptophan in HSA (Figure 2). In the absence of prodan, intrinsic tryptophan of HSA displayed typical emission spectrum with emission maxima around 340 nm. Binding of prodan to HSA did not alter the emission maxima and the contour of the Trp-214 emission spectrum; however, prodan decreased the fluorescence intensity of tryptophan in a concentration-dependent manner with concomitant increase in bound prodan fluorescence. In addition, the binding of prodan to HSA did not perturb the CD spectra of HSA in the range of 200 to 300 nm (*38*), indicating that the incorporation of the label did not lead to any significant change in the secondary structure of the protein. Taking together, the data indicated that the quenching of the tryptophan fluorescence was due to nonradiative energy transfer between Trp-214 and prodan rather than direct perturbation of the environment of the flurophore.

The decrease in the donor (Trp-214) fluorescence intensity was used to calculate the efficiency of the energy transfer, and Förster's theory of dipole−dipole energy transfer was used to determine the distance between Trp-214 and prodan (Experimental Procedures). The emission at 340 nm for HSA labeled with prodan (30 μM) was quenched by ~50% compared to the emission of the native protein. The efficiency of transfer was calculated using eq 4 and was

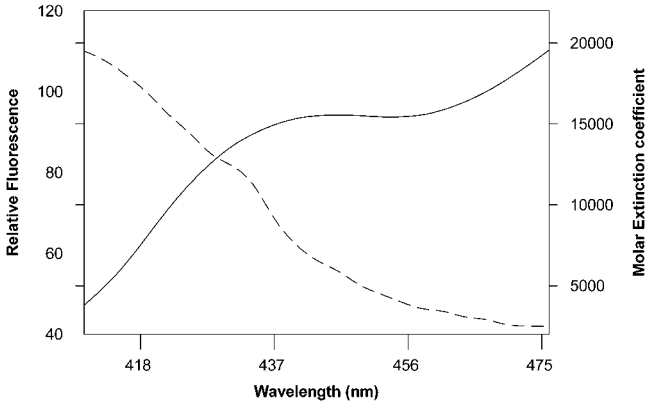

FIGURE 3: Overlaps between the absorption spectrum of CM (- - -) and the fluorescence emission spectrum of HSA−prodan (—) when excited at 360 nm. The CM-HSA absorption spectrum was recorded in 20 mM phosphate buffer, pH 7.0.

corrected for the acceptor stoichiometry. The Förster distance (R_o) between Trp-214 and prodan was calculated to be 25.7 ± 0.6 Å. The corrected efficiency of energy transfer between Trp-214 and prodan moiety at the drug site 1 was 47−50%, and the mean distance between the two residues was calculated to be 25.5 ± 0.5 Å. All distances reported are the averages of three identical experiments.

Distance Between Trp-214 and Cys-34. The distance between the single sulfhydryl group, Cys-34 located at domain I, and Trp-214 located in domain II was measured with the goal of using the interdomain distance to monitor conformational changes upon ligand binding and unfolding of HSA. The CM-labeled HSA (CM-HSA) was prepared as described under Experimental Procedures. Under the conditions used, 0.97 mol of CM was incorporated per mole of HSA. The CM-HSA and unlabeled HSA produced identical CD spectra, indicating that the labeling of HSA by CM did not alter the secondary structure of HSA (data not shown). In addition, the incorporation of CM did not alter the binding of palmitic acid or prodan to HSA (data not shown). The fluorescence emission spectrum of Trp-214 and the absorbance spectrum of CM-HSA are shown in Figure 2. The position of the emission maximum and shape of the tryptophan emission spectrum of HSA were not perturbed due to incorporation of CM (data not shown). However, incorporation of CM at Cys-34 decreased the intrinsic tryptophan fluorescence of HSA by ~30%. R_o was calculated to be 30.1 ± 0.7 Å. The efficiency of transfer was in the order of 33−35%, and the mean distance between the Trp-214 and CM at Cys-34 was calculated to be 33.1 ± 0.8 Å. The interdomain distance between Trp-214 of domain II and Cys-34 of domain I measured in this report using CM labeled Cys-34 is in good agreement with the earlier determined FRET distance of 35.1 ± 0.8 Å between azomercurial modified Cys-34 and Trp-214 (*31*).

Distance Between Cys-34 and Prodan Binding Site. HSA was labeled with CM and prodan simultaneously to measure the distance between Cys-34 and the bound prodan moiety. As shown in Figure 3, the spectral overlap of the fluorescence emission spectrum of the HSA−prodan complex and the absorbance spectrum of CM-HSA is ideal for fluorescence energy transfer measurements. The fluorescence intensity of the donor (HSA bound prodan) was reduced in the presence of acceptor CM, which was covalently bound to HSA.

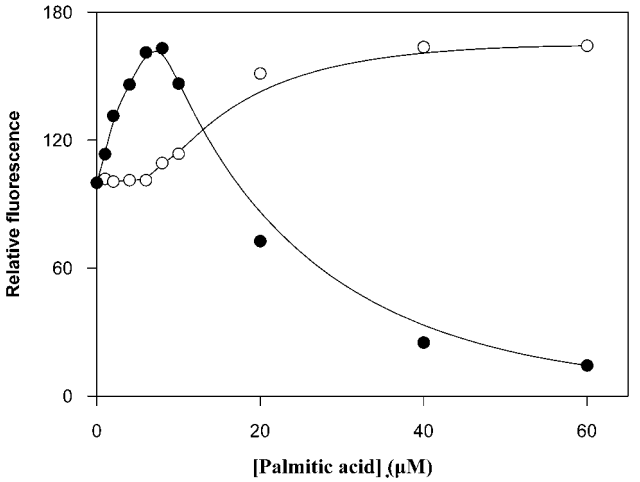

FIGURE 4: Effects of palmitic acid on the intrinsic tryptophan fluorescence of HSA (○) and prodan fluorescence (●). HSA (10 μM) was incubated with a large excess of prodan (200 μM) at 25 °C for 30 min to form the HSA−prodan complex. HSA (1 μM) and HSA−prodan (1 μM HSA) were incubated with a range of palmitic acid concentrations (1−60 μM) at 25 °C for 30 min. The excitation and emission wavelengths were 295 and 340 nm for tryptophan and 360 and 445 nm for prodan, respectively.

Incorporation of CM at Cys-34 reduced the bound prodan fluorescence at 445 nm by ~40% with a concomitant increase of CM emission at 480 nm. The R_o was calculated to be 30.1 ± 0.4 Å and the mean distance between the bound prodan and CM-Cys-34 was determined to be 32.5 ± 0.8 Å.

Binding of Palmitic Acid to HSA. We studied the interaction of palmitic acid with HSA by two different approaches. In the first approach, we used environment-sensitive prodan fluorescence to probe the binding of palmitic acid to HSA. Low concentrations of palmitic acid (1−10 μM) increased the bound prodan fluorescence without altering the fluorescence intensity of free prodan at 520 nm. For example, 6 μM palmitic acid increased the bound prodan fluorescence by 65% (Figure 4). Low concentrations of palmitic acid did not change the free prodan fluorescence in the absence of HSA (data not shown). Thus, the increase in bound prodan fluorescence in the presence of low concentration of palmitic acid could be attributed to a change in the quantum yield of the bound prodan rather than due to enhanced binding. To further test this idea, HSA−prodan complex was formed by incubating 1 μM prodan with 50 μM of HSA for 30 min. Under this condition, the free prodan concentration was negligible (data not shown). Addition of 8 μM palmitic acid to this complex increased the bound prodan fluorescence by 55%, demonstrating that the increase in bound prodan fluorescence was due to an increase in the quantum yield of HSA bound prodan. The results indicate that palmitic acid in low concentration induces conformational change in the prodan binding site of HSA.

However, high concentrations of palmitic acid (>10 μM) decreased bound prodan fluorescence with concomitant increase in free prodan fluorescence. For example, 40 μM palmitic acid decreased the bound prodan fluorescence by 75%, indicating that the binding of palmitic acid at the low affinity sites displaces prodan from HSA (Figure 4). Taking together, the results indicated the presence of at least two affinity classes of binding sites for palmitic acid on HSA;

one of high affinity and other of low affinity. However, no attempt had been made to identify number of low and high affinity binding sites.

In the second approach, we used the intrinsic tryptophan fluorescence of HSA to monitor the palmitic acid binding. Low concentrations of palmitic acid (1−10 μM) did not change the tryptophan fluorescence but on increasing the concentrations of palmitic acid beyond 10 μM, the tryptophan fluorescence increased in a concentration-dependent fashion. As shown in Figure 4, in the presence of 6 μM palmitic acid, the tryptophan fluorescence change was about only 1%, but in the presence of 40 μM palmitic acid, the fluorescence intensity increased by 64% (Figure 4). The data suggested that the high affinity binding site(s) are located close to the prodan binding region, away from Trp-214, while some of the low affinity sites on domain II are located in the vicinity of Trp-214.

In addition, the acrylamide quenching of Trp-214 yielded the same Stern−Volmer quenching constant (6.1 M^{-1}) in the absence or presence of 5 μM palmitic acid, indicating that the immediate environment of Trp-214 was not perturbed by 5 μM palmitic acid. Also, the CD spectra of HSA in the range of 190 to 260 nm showed no significant difference in the absence and presence of 5 μM palmitic acid, indicating that no detectable change occurs in the secondary structure of HSA in the presence of 5 μM of palmitic acid (data not shown). However, 5 μM palmitic acid decreased the efficiency of energy transfer between Trp-214 and CM incorporated at Cys-34 by 15%. The data indicated that the interdomain distance increased by 4.4 Å from 33.1 ± 0.8 to 37.5 ± 1 Å. Thus, a low concentration of palmitic acid (5 μM) increased the interdomain distance between domain II and domain I without perturbing the immediate environment of tryptophan flurophore.

Chemical Denaturation Studies. The intrinsic tryptophan fluorescence and the bound prodan fluorescence were used to monitor the kinetics of unfolding of HSA. The bound prodan fluorescence at 445 nm decreased instantaneously on addition of the denaturant to HSA−prodan complex. Fluorescence of HSA−prodan complex was reduced by 60 and 95% within the dead time of measurement (~10 s) in the presence of 2 and 6 M GdnHCl, respectively. Interestingly, there was no further loss of prodan fluorescence with time beyond the initial loss (Figure 5A). A steady state fluorescence spectrophotometer did not permit determination of the dissociation rate constant of HSA−prodan complex in the presence of denaturant because the dissociation occurred within the dead time of the experiment. In the second approach, the decrease in tryptophan fluorescence with time in the presence of the denaturant was monitored as a measure of unfolding kinetics. In contrast to the rapid loss of prodan fluorescence, tryptophan fluorescence showed a single exponential decay. In the presence of the 6 M GdnHCl, 50% of the maximum fluorescence change occurred in 40 min. Our data indicated that GdnHCl induces a rapid unfolding of the prodan binding region, while the local environment of Trp214 unfolds slowly (Figure 5A). The differential effects of GdnHCl on Trp-214 and prodan fluorescence suggested that the unfolding of domain II occurred in a stepwise manner.

To investigate the unfolding equilibria, HSA−prodan complex was mixed with varying concentrations of GdnHCl and incubated for 1 h to allow equilibration. GdnHCl decreased the bound prodan fluorescence in a concentration-dependent manner with concomitant increase in free prodan fluorescence at 520 nm. The fluorescence data were fitted using a two-state transition model and a three-state transition model (Experimental Procedures). Fits for the three-state model increased the Chi^2 and will not be used for further discussion. Figure 5B represents the fit of the unfolding data to a two-state model. The equilibrium unfolding transition from the native state to denatured state was found to be a single-step process with no detectable intermediate state. The nonlinear regression analysis of the data yielded the value of ΔG°_U and m. Dividing ΔG°_U by the slope (m) gives an approximate value for the midpoint of unfolding transition, called $D_{50\%}$. $D_{50\%}$ was calculated to be 2.15 ± 0.5 M GdnHCl (ΔG°_U = 20.3 ± 1.5 kJ mol^{-1}, m = 9.2 ± 1.0). This fits well

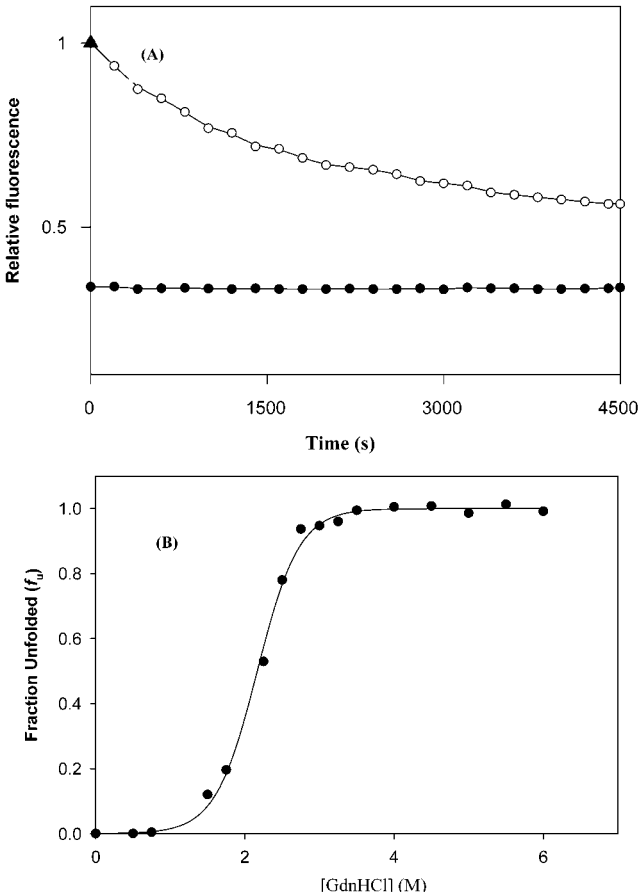

FIGURE 5: GdnHCl-induced unfolding of HSA. (A) Kinetics of unfolding of HSA monitored by intrinsic tryptophan fluorescence (○) and prodan fluorescence (●). The ▲ represents prodan fluorescence in the absence of GdnHCl. Unfolding of prodan site occurred in the dead time of the experiment and the observed trace shows the change in fluorescence of prodan as a function of time. The solid line through the tryptophan fluorescence data is a nonlinear least-squares fit of single-exponential decay. (B) Equilibrium unfolding curve of HSA monitored by bound prodan fluorescence. HSA (10 μM) was incubated with large excess of prodan (200 μM) at 25 °C for 30 min to form the HSA−prodan complex. HSA−prodan (1 μM HSA) in 20 mM phosphate buffer (pH-7.0) was incubated at 25 °C for 1 h with different concentrations of GdnHCl (0.5−6 M). The excitation and the emission wavelengths were 360 and 445 nm, respectively. The fraction unfolded at different concentrations of GdnHCl was calculated as described in Experimental Procedures. The solid line through the data is a nonlinear least-squares fit to eq 9.

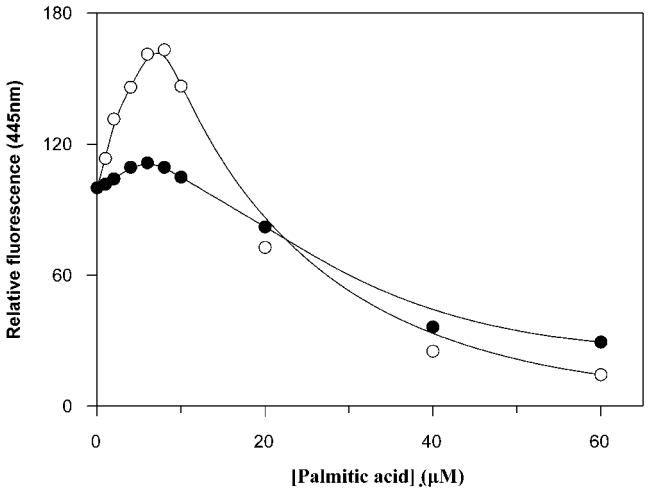

FIGURE 6: Effects of GdnHCl on palmitic acid binding. The changes in prodan fluorescence in the absence (○) and presence (●) of 2 M GdnHCl were determined at 25 °C. The excitation and emission wavelengths were 360 and 445 nm.

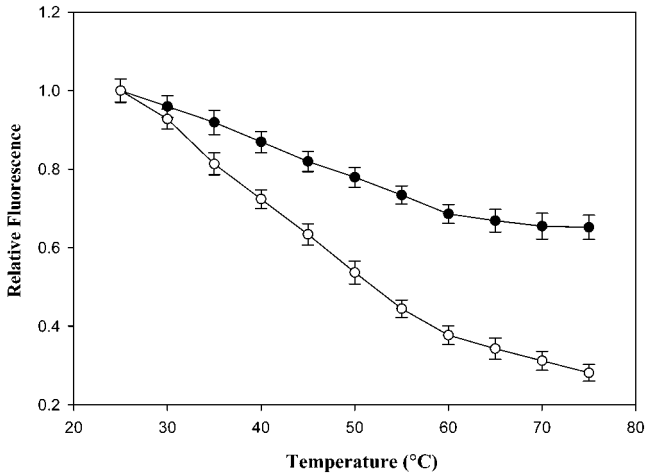

FIGURE 7: Thermal denaturation of HSA followed by intrinsic tryptophan fluorescence (●) and bound prodan fluorescence (○). HSA (1 μM) and HSA−prodan complex (1 μM HSA) complex in 20 mM phosphate buffer (pH 7.0) were heated in continuous fashion and fluorescence was recorded at different temperatures ranging from 25 to 80 °C after incubating the sample for 10 min. The excitation and the emission wavelengths were 295 and 340 nm for tryptophan and 360 and 445 nm for prodan.

with earlier reports that chemical denaturation of HSA, as monitored by fluorescence of the lone tryptophan in domain II, followed a single-step transition (*20*, *21*).

In the presence of a low concentration of the GdnHCl (2 M), the transfer efficiency between Trp-214 and CM-labeled Cys-34 decreased by 10%, indicating that the interdomain distance was increased by 2.7 ± 0.6 Å. We also determined the effects of GdnHCl on palmitic acid binding. In the presence of 2 M GdnHCl, low concentrations of palmitic acid did not change the prodan fluorescence, whereas relatively high concentrations of palmitic acid decreased the prodan fluorescence indicating that 2 M GdnHCl selectively abolished the high affinity palmitic acid binding site on HSA, while the low affinity sites were not affected (Figure 6). However, at high concentrations of GdnHCl, binding of palmitic acid at both the high affinity and low affinity sites were abolished (data not shown). Thus, at low concentrations of GdnHCl, the structure of HSA is not completely lost as evident from the selective loss of the ligand binding.

Thermal Unfolding Studies. Temperature induced unfolding of HSA was monitored by measuring the intrinsic tryptophan fluorescence and extrinsic prodan fluorescence. The prodan fluorescence decreased in a sigmoidal fashion with increasing temperature (Figure 7). The tryptophan fluorescence−temperature curve (Figure 7) also followed a similar trend. The temperature at the midpoint of denaturation (T_M) was calculated by nonlinear regression analysis of the fluorescence data, using a two-state model (*22*). The T_M of the prodan unfolding transition was 48.3 ± 0.7 °C and that of the tryptophan−temperature curve was calculated to be 59.4 ± 0.8 °C. Thus, the T_M values determined using two different probes differed considerably, and the thermal unfolding of prodan binding site preceded the melting of the Trp-214 environment reflecting differential unfolding of domain II. Previously, a T_M value of 63.1 ± 0.4 °C was reported for HSA using a differential scanning calorimeter (*49*), which is similar to the T_M value obtained using intrinsic tryptophan fluorescence of HSA (Figure 7 and refs *18* and *49*), suggesting that the T_M value obtained using Trp-214 fluorescence may reflect the global melting of HSA.

DISCUSSION

Intra and Interdomain FRET Measurements. In the present study, we determined the intradomain distance between prodan and Trp-214 in domain II to be 25.5 ± 0.5 Å. Prodan has been shown to bind in the drug site I of HSA (*38*); thus, our data indicate that the distance between drug site I (warfarin site) and Trp-214 is 25.5 ± 0.5 Å. The Cys-34 of domain I was covalently labeled with CM to produce an acceptor for both Trp-214 and prodan fluorescence. The CM labeling did not perturb the secondary structure of HSA, tryptophan environment, and the ligand binding properties of HSA, indicating that the CM-HSA could be used as a fluorescent tool to characterize the protein. The FRET distance between Trp-214 and CM-labeled Cys-34 residues was measured to be 33.1 ± 0.8 Å, and the distance between prodan and CM-labeled Cys-34 was measured to be 32.4 ± 1 Å. The crystal structures of unliganded HSA and of HSA complexed with warfarin have been solved recently (*50*, *51*). On the basis of the crystal structures, we calculated the distances between Trp-214 and Cys-34 residues and warfarin moiety at the drug site 1 and Cys-34 using Swiss-PdbViewer (Version 3.6b3) to be ∼33 and ∼32.5 Å, respectively. The calculated distances were in excellent agreement with the FRET measured distances, indicating that the FRET distances could be used to determine the effects of ligand binding on the domain movements of HSA and to understand the protein unfolding process. The distance measured by FRET technique is a time-averaged distance of the dynamic solution structure of the protein in comparison to the distance from a static model determined from the crystallographic data. The results of the distance measurements combined with various palmitic acid binding sites from the literature are summarized on the schematic model of HSA drawn in Figure 8. The planar representation of the protein molecule helps to visualize the spatial mapping of Trp-214, Cys-34, and the prodan binding site.

Palmitic Acid Binding Sites on HSA and Conformational Changes. The crystal structure of HSA complexed with

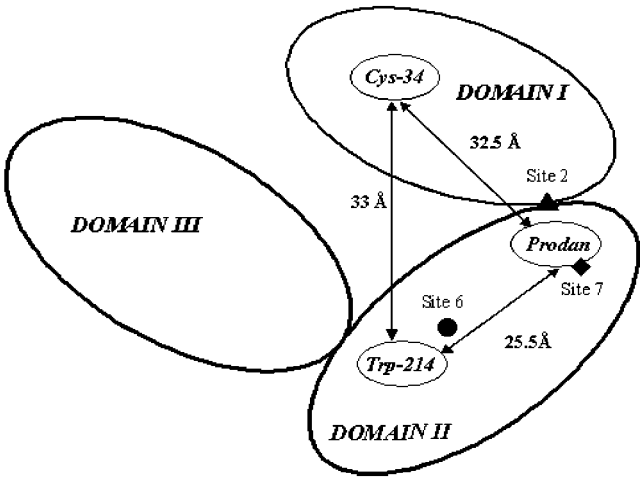

FIGURE 8: A two-dimensional schematic diagram of the relative locations of bound prodan, Trp-214, and Cys-34 on HSA was constructed on the basis of FRET distance measurements. The HSA subunits were drawn from the deduced crystal structure of the unliganded HSA (*50*). The palmitic acid binding site 2 (▲), site 6 (●), and site 7 (◆) are modeled on the basis of the crystal structure of the HSA liganded to fatty acid (*8*). The palmitic acid binding site 2 is the high affinity site located in the interface of domain IA and IIA, while site 6 is in the interface of domain IIA and IIB, and site 7 is in the interior of domain II; overlapping with the prodan binding site are low affinity palmitic acid binding sites.

palmitate revealed the presence of seven fatty acid binding sites on HSA. These binding sites are distributed asymmetrically in HSA: a single site in domain IB, one site in domain IIA, two sites in domain IIIA, one site in domain IIIB, and two binding sites in the interface of subdomains IA−IIA and IIA−IIB, respectively (*7*, *8*). However, the major unresolved issue is the identity of the high affinity and low affinity palmitic acid binding sites in HSA.

Low concentrations of palmitic acid did not alter the Trp-214 fluorescence, whereas the bound prodan fluorescence increased under same conditions indicating that the high affinity-binding site for the palmitic acid is located in the vicinity of the prodan binding region (Figure 4). The fatty acid binding site 2 is located in the interface of subdomains IA and IIA (Figure 8), close to the hydrophobic cleft forming the drug-binding site I (*7*). Binding of fatty acids at this site is thought to induce conformational change in the protein as this site is dislocated into two-half-sites in defatted HSA and the formation of a contiguous pocket to accommodate the fatty acid requires rotation of domain I relative to domain II (*7*, *52*). This is a possible explanation for the observed increase in the interdomain distance between Trp-214 and Cys-34 by 5 Å in the presence of 5 μM palmitic acid. Further, our observation that the low concentration of palmitic acid enhanced the fluorescence of HSA bound prodan without decreasing the free prodan fluorescence is consistent with the idea that conformational changes that occurred upon binding of fatty acid at site 2 increases the hydrophobicity of the drug binding site I (*51*). Taken together, our results indicate that fatty acid binding site 2 is one of the high affinity fatty acid binding sites in HSA.

At high concentrations of palmitic acid, the bound prodan fluorescence decreased with a concomitant increase in free prodan fluorescence. This observation is probably attributable to direct competition between the probe and fatty acid for binding to the hydrophobic pocket in IIA. This interpretation is supported by the observation that fatty acid binding site 7 as shown in Figure 8 overlaps the drug site 1 (*8*). The fatty acid binds to this site (designated site 7) in a manner that is suggestive of a low affinity interaction primarily caused by nonspecific interactions between the protein and the fatty acid carboxylate group (*8*). Similarly, the increase in Trp-214 fluorescence in the presence of high concentrations of palmitic acid could be correlated to the interaction of fatty acid at binding site 6. Site 6 is located at the interface of subdomain IIA and IIB and is in close proximity of Trp-214 (Figure 8) (*51*). The binding of fatty acid at site 6 induces local conformational changes that perturb the immediate environment of Trp-214. These observations suggest that the fatty acid binding sites 6 and 7, located in the interior of domain II, are low affinity sites.

Unfolding Studies. In this study, using prodan fluorescence we found that GdnHCl-induced denaturation of HSA followed a single-step transition. Similar observations were made using the intrinsic tryptophan fluorescence (*20*, *21*). However, the kinetics of unfolding of the Trp-214 environment was markedly different from the prodan site in HSA. The prodan fluorescence decreased instantaneously, within the dead time of measurement, and then remained unchanged over the period of observation, while the Trp-214 fluorescence showed a single-exponential decay (Figure 5A). The rate of decrease of prodan fluorescence was several hundred times faster than that of rate of decrease of tryptophan fluorescence. This differential rate of decrease in fluorescence of Trp-214 and prodan reflects the stepwise unfolding of domain II with unfolding of prodan binding site preceding the unfolding of the tryptophan environment. Further, thermal denaturation of HSA measured by fluorescence−temperature curves of bound prodan and tryptophan produced unfolding temperatures of 48.3 ± 0.7 and 59.4 ± 0.8 °C for prodan and tryptophan, respectively, indicating differential unfolding of domain II. The data suggest that a part of domain IIA that corresponds to the environment of Trp-214 contains tertiary structure, which is more resistant to thermal denaturation than the prodan site.

FRET analysis at low concentration of GdnHCl (2 M) suggested that the separation distance between domains I and II increased during the unfolding process. Further, low concentration of GdnHCl (2 M) selectively inhibited the binding of palmitic acid at the high affinity site while binding at the low affinity sites was not affected (Figure 6). However, at high concentrations of GdnHCl (5 M), the binding of palmitic acid at both high and low affinity sites was lost (data not shown). The most likely explanation for this differential loss of binding of palmitic acid is that the initial separation of domains I and II at low concentrations of GdnHCl disrupts the high affinity site/s located at the interface of domain I and II, while the low affinity binding sites located in the interior of the domain II are not affected. However, at high concentrations of GdnHCl, all palmitic acid binding sites are abolished as a result of complete unfolding of the domains. Flora et al. (1998) also found that the interdomain distance between Trp-214 and acrylodan labeled Cys-34 increased in the presence of low concentrations of GdnHCl (*22*). In addition, the mean residue ellipticity signal was not significantly altered at 2 M GdnHCl (*21*). These data along with the instantaneous loss of prodan binding supports the idea that the unfolding of HSA occurs with an

initial separation of domain I and domain II resulting in the expanded form of the protein followed by complete unfolding of the domains.

The information obtained from a single probe such as tryptophan or prodan is not often sufficient to characterize the changes in different domains of proteins. Further, fluorescence probes reflect the average properties of all forms of protein, and it might not be possible to differentiate among the native, intermediate, and unfolded forms of the protein. The inherent presumption in a two-state model that only two states exist in equilibrium might appear aberrant when the energy landscape existing between the native and unfolded forms of a multidomain protein such as HSA is complex and folding intermediates might be expected to accumulate. In this study, using multiple probes, we found that GdnHCl-induced unfolding of HSA occurred through an incremental loss of structure. There was an initial domain separation resulting in the expanded form of the protein followed by complete unfolding of the domains at high denaturant concentration. It appears that the protein unfolds with progressively changing structure rather than by a strict two-state mechanism. Recently, incremental unfolding of a relatively small protein barstar has been reported using time-resolved FRET (*53*) although urea-induced unfolding of barstar was shown to occur through the formation of at least two unfolding intermediates (*54*). Thus, it might be desirable to use multiple probes for characterization of multidomain proteins particularly when each domain can undergo the folding process relatively independent of the other domains.

ACKNOWLEDGMENT

We thank Dr. Leslie Wilson, Dr. Richard Himes, and Dr. Nand Kishore for critical reading of the manuscript.

REFERENCES

1. He, X. M., and Carter, D. C. (1992) Atomic structure and chemistry of human serum albumin. *Nature 358*, 209−215.
2. Carter, D. C., and Ho, J. X. (1994) Structure of serum albumin. *Adv. Protein Chem. 45*, 152−203.
3. Sudlow, G., Brikket, D. J., and Wade, D. N. (1975) The characterization of two specific drug binding sites on human serum albumin. *Mol. Pharmacol. 11*, 824−832.
4. Sjoholm, I., Ekman, B., Kober, A., Ljungstedt-Pahlman, I., Seiving, B., and Sjodin, T. (1979) Binding of drugs to human serum albumin. XI. The specificity of three binding sites as studied with albumin immobilized in microparticles. *Mol. Pharmacol. 16*, 767−777.
5. Kragh-Hansen, U. (1988) Evidence for a large and flexible region of human serum albumin possessing high affinity binding sites for salicylate, warfarin, and other ligands. *Mol. Pharmacol. 34*, 160−171.
6. Yamasaki, K., Maruyama, T., Kragh-Hansen, U., and Otagiri, M. (1996) Characterization of drug binding site 1 on human serum albumin: concept about the structure of a drug-binding site *Biochim. Biophys. Acta*, *1295*, 147−157.
7. Curry, S., Mandelkow, H., Brick, P., and Franks, N. (1998) Crystal structure of human serum albumin complexed with fatty acid reveals an asymmetric distribution of binding sites. *Nat. Struct. Biol. 5*, 827−835.
8. Bhattacharya, A. A., Grüne, T., and Curry, S. (2000) Crystallographic analysis reveals common modes of binding of medium and long-chain fatty acids to human serum albumin. *J. Mol. Biol. 303*, 721−732.
9. Ashbrook, J. D., Spector, A. A., Santos, E. C., and Fletcher, J. E. (1972) Long chain fatty acid binding to human plasma albumin. *J. Biol. Chem. 247*, 7038−7042.
10. Kragh-Hansen, U. (1981) Molecular aspects of ligand binding to serum albumin. *Pharmacol. Rev. 33*, 17−54.
11. Grundy, S. M., and Denke, M. A. (1990) Dietary influences on serum lipids and lipoproteins. *J. Lipid. Res. 7*, 1149−1172.
12. Narazaki, R., Maruyama, T. and Otagiri, M. (1997) Probing the Cysteine-34 residue in human serum albumin by fluorescent techniques. *Biochim. Biophys. Acta 1338*, 275−281.
13. Wetlaufer, D. B. (1981) Folding of protein fragments. *Adv. Protein Chem. 34*, 61−92.
14. Jaenicke, R., and Seckler, R. (1997) Protein misassembly in vitro. *Adv. Protein Chem. 50*, 1−59.
15. King, T. P., and Spencer, M. (1970) Structural studies and organic ligand-binding properties of bovine plasma albumin. *J. Biol. Chem. 245*, 6134−6148.
16. Reed, R. G., Feldhoff, R. C., Clute, O. L., and Peters, T., Jr. (1975) Fragments of bovine serum albumin produced by limited proteolysis − Conformation and ligand binding. *Biochemistry 14*, 4578−4583.
17. Kjeldsen, T., Pettersson, A. F., Drube, L., Kurtzhals, P., Jonassen, I., Havelund, S., Hansen, P. H., and Markussen, J. (1998) Secretory expression of human albumin domains in *Saccharomyces cerevisiae* and their binding of myristic acid and an acylated insulin analogue. *Prot. Express. Purif. 13*, 163−169.
18. Picó, G. (1995) Thermodynamic aspects of the thermal stability of human serum albumin. *Biochem. Mol. Biol. Int. 36*, 1017−23.
19. Muzammil, S., Kumar, Y., and Tayyab, S. (1999) Molten globule-like state of human serum albumin at low pH. *Eur. J. Biochem. 266*, 26−32.
20. Tayyab, S., Siddiqui, M. U., and Ahmad, N. (1995) Experimental determination of the free energy of unfolding of proteins *Biochem. Ed. 23*, 162−164.
21. Muzammil, S., Kumar, Y., and Tayyab, S. (2000) Anion-induced stabilization of human serum albumin prevents the formation of intermediate during urea denaturation *Proteins: Struct. Funct. Genet. 40*, 29−38.
22. Flora, K., Brennan, J. D., Baker, G. A., Doody, M. A., and Bright, F. V. (1998) Unfolding of acrylodan-labeled human serum albumin probed by steady state and time-resolved fluorescence methods. *Biophys. J. 75*, 1084−1096.
23. Brown, J. R. (1977). Serum albumin: amino acid sequence. In *Albumin Structure, Function and Uses* (Rosenoer, V. M., Oratz, M., and Rothschild, M. A., Eds.) pp 27−51, Pergamon, Oxford.
24. Berde, C. B., Hudson, B. S., Simoni, R. D., and Sklar, L. A. (1979) Human serum albumin spectroscopic studies of binding and proximity relationship for fatty acids and bilirubin. *J. Biol. Chem. 254*, 391−400.
25. Farruggia, B., Garcia, F., and Picó, G. (1995) Structural features of the hydroxy- and keto disubstituted bile salts: human serum albumin binding. *Biochim. Biophys. Acta 1252*, 59−68.
26. Nerli, B., Romanini, D., and Picó, G. (1997) Structural specificity requirements in the binding of beta lactam antibiotics to human serum albumin. *Chem. Biol. Interact. 104*, 179−202.
27. Lakowicz, J. R. (1999) *Principles of Fluorescence Spectroscopy*, 2nd ed., Kluwer Academic/Plenum Publishers, New York.
28. Panda, D., Roy, S., and Bhattacharyya, B. (1992) Reversible dimer dissociation of tubulin S and tubulin detected by fluorescence anisotropy. *Biochemistry 31*, 9709−9716.
29. Deniz, A. A., Laurence, T. A., Beligere, G. S., Dahan, M., Martin, A. B., Chemla, D. S., Dawson, P. E., Schultz, P. G., and Weiss, S. (2000) Single-molecule protein folding diffusion fluorescence resonance energy transfer studies of the denaturation of chymotrypsin inhibitor 2. *Proc. Natl. Acad. Sci. U.S.A. 97*, 5179−84.
30. Mukhopadhyay, J., Kapanidis, A. N., Mekler, V., Kortkhonjia, E., Ebright, Y. W., and Ebright, R. H. (2001) Translocation of sigma (70) with RNA polymerase during transcription: fluorescence resonance energy transfer assay for movement relative to DNA. *Cell 106*, 453−63.

31. Suzukida, M., Le, H. P., Shahid, F., McPherson, R. A., Birnbaum, E. R., and Darnall, D. W. (1983) Resonance energy transfer between cysteine-34 and tryptophan-214 in human serum albumin-distance measurements as a function of pH. *Biochemistry 22*, 2415−2420.
32. Weber, G., and Farris, F. J. (1979) Synthesis and spectral properties of a hydrophobic fluorescent probe: 6-propionyl-2-(dimethylamino) naphthalene *Biochemistry 18*, 3075−3078.
33. MacGregor, R. B., and Weber, G. (1986) Estimation of polarity of protein interior by optical spectroscopy. *Nature 319*, 70−73.
34. Cowley, D. J. (1986) Polar pocket with nonpolar lining. *Nature 319*, 14−15
35. Panda, D., Miller, H. P., Islam, K., and Wilson, L. (1997) Stabilization of microtubule dynamics by estramustine by binding to a novel site in tubulin: A possible mechanistic basis of its antitumor action. *Proc. Natl. Acad. Sci. U.S.A. 94*, 10560−10564.
36. Panda, D., Singh, J. P., and Wilson, L. (1997) Suppression of microtubule dynamics by LY290181: A potential mechanism for its antiproliferative action, *J. Biol. Chem. 272*, 7681−7687.
37. Panda, D., Ananthnarayan, V., Larson, G., Shih, C., Jordan, M. A., and Wilson, L. (2000) Interaction of the antitumor compound cryptophycin-52 with tubulin *Biochemistry 39*, 14121−14127.
38. Moreno, F., Cortijo, M., and Jiménez, J. G. (1999) The fluorescent probe prodan characterizes the warfarin-binding site on human serum albumin. *Photochem. Photobiol. 69*, 8−15.
39. Mas, M. T., and Coleman, R. F. (1985) Spectroscopic studies of interaction of coenzymes and coenzyme fragments with pig heart, oxidized triphosphopyridine nucleotide specific isocitrate dehydrogenase. *Biochemistry 24*, 1634−1646.
40. Horowitz, P. M., and Criscimagna, N. L. (1985) Differential binding of the fluorescent probe 8-anilinonaphthalene-2-sulfonic acid to rhodanese catalytic intermediates. *Biochemistry 24*, 2587−2593.
41. Moreno, F., Cortijo, M., and Jiménez, J. G. (1999) Interaction of acrylodan with human serum albumin. A fluorescence spectroscopic study. *Photochem. Photobiol. 70*, 695−700.
42. Moreno, F., and Jiménez, J. G. (1999) Binding of Promen fluorescent probe to human serum albumin. A fluorescence spectroscopic study. *Chem.-Biol. Interact. 121*, 237−252.
43. Bradford, M. M. (1976) A rapid and sensitive method for the quantitation of microgram quantities of protein utilizing the principle of protein-dye binding. *Anal. Biochem. 72*, 248−54.
44. Wu, P., and Brand, L. (1994) Resonance energy transfer: methods and applications. *Anal. Biochem. 218*, 1−13.
45. Stryer, L. (1978) Fluorescence energy transfer as a spectroscopic ruler. *Annu. Rev. Biochem. 40*, 83−114.
46. Fairclough, R. H., and Cantor, C. R. (1978) The use of singlet−singlet energy transfer to study macromolecular assemblies. *Methods Enzymol. 48*, 347−379.
47. Wu, F. Y., and Tyagi, S. C. (1987) Fluorescence resonance energy transfer studies on the proximity relationship between the intrinsic metal ion and substrate binding sites of *Escherichia coli* RNA polymerase. *J. Biol. Chem. 262*, 13147−13154.
48. Santoro, M., and Bolen, D. W. (1988) Unfolding free energy changes determined by linear extrapolation method. 1. Unfolding of phenylmethanesulfonyl α-chymotrypsin using different denaturants. *Biochemistry 27*, 8063−8068.
49. Picó, G. (1997) Thermodynamic features of thermal unfolding of human serum albumin. *Int. J. Biol. Macromol. 20*, 63−73.
50. Sugio, S., Kashima, A., Mochizuki, S., Noda, M., and Kobayashi, K. (1999) Crystal structure of human serum albumin at 2.5 Å resolution. *Protein Eng. 6*, 439−446.
51. Petitpas, I., Bhattacharya, A. A., Twine, S., East, M., and Curry, S. (2001) Crystal structure analysis of warfarin binding to human serum albumin − Anatomy of drug site 1. *J. Biol. Chem. 276*, 22804−22809.
52. Curry, S., Brick, P., and Franks, N. P. (1999). Fatty acid binding to human serum albumin: New insights from crystallographic studies. *Biochim. Biophys. Acta 1441*, 131−140.
53. Lakshmikanth, G. S., Sridevi, K., Krishnamoorthy, G., and Udgaonkar, J. B. (2001) Structure is lost incrementally during the unfolding of barstar *Nat. Struct. Biol. 8*, 199−804.
54. Zaidi, F. N., Nath, U., and Udgaonkar, J. B. (1997) Multiple intermediates and transition states during protein unfolding. *Nat. Struct. Biol. 4*, 1016−1024.

BI025699V